NeuroImage 234 (2021) 117973

Contents lists available at ScienceDirect

NeuroImage

journal homepage: www.elsevier.com/locate/neuroimage

High temporal resolution functional magnetic resonance spectroscopy in the mouse upon visual stimulation

Clémence Ligneul, Francisca F. Fernandes, Noam Shemesh*

Champalimaud Research, Champalimaud Centre for the Unknown, Av. Brasilia, Lisbon 1400-038, Portugal

A B S T R A C T

Functional magnetic resonance spectroscopy (fMRS) quantifies metabolic variations upon presentation of a stimulus and can therefore provide complementary information compared to activity inferred from functional magnetic resonance imaging (fMRI). Improving the temporal resolution of fMRS can be beneficial to clinical applications where detailed information on metabolism can assist the characterization of brain function in healthy and sick populations as well as for neuroscience applications where information on the nature of the underlying activity could be potentially gained. Furthermore, fMRS with higher temporal resolution could benefit basic studies on animal models of disease and for investigating brain function in general. However, to date, fMRS has been limited to sustained periods of activation which risk adaptation and other undesirable effects. Here, we performed fMRS experiments in the mouse with high temporal resolution (12 s), and show the feasibility of such an approach for reliably quantifying metabolic variations upon activation. We detected metabolic variations in the superior colliculus of mice subjected to visual stimulation delivered in a block paradigm at 9.4 T. A robust modulation of glutamate is observed on the average time course, on the difference spectra and on the concentration distributions during active and recovery periods. A general linear model is used for the statistical analysis, and for exploring the nature of the modulation. Changes in NAAG, PCr and Cr levels were also detected. A control experiment with no stimulation reveals potential metabolic signal "drifts" that are not correlated with the functional activity, which should be taken into account when analyzing fMRS data in general. Our findings are promising for future applications of fMRS.

Introduction

The complexity of brain function calls for diverse and complementary approaches for reporting on different aspects of neural activity. Functional magnetic resonance imaging (fMRI) is one of the most popular noninvasive techniques capable of studying human brain activity from a global brain perspective and with relatively high spatial resolution. Relying on neurovascular couplings as surrogate reporters for activity (Logothetis et al., 2001), fMRI can identify brain areas involved in a given task or in processing information. At higher fields, Blood Oxygen Level Dependent (BOLD) fMRI even allows for laminar resolution (Polimeni et al., 2010; Goense et al., 2012), and, to some extent, specificity and insight into how the brain processes stimuli and integrates information.

Despite its invaluable contributions to cognitive neuroscience and to clinical applications, BOLD fMRI is typically hampered in terms of *specificity*, mainly because of its indirect nature (Logothetis, 2008). For example, excitation and inhibition balances or neuromodulatory effects cannot be specifically inferred from (typical) BOLD responses, because the neurovascular coupling mechanisms governing each of these effects is not yet fully understood (Logothetis, 2008).

Magnetic resonance spectroscopy (MRS) can provide noninvasive information on myriad molecules involved in brain metabolism if they are sufficiently concentrated (~mM) *in vivo*, thus endowing MRS with some degree of specificity. Certain metabolites are concentrated in particular cell types (Urenjak et al., 1993; Belle et al., 2002; Griffin et al., 2002), making MRS more specific towards intracellular space compared to its water-driven MRI counterpart. Particularly interesting perhaps are MRS's capabilities of detecting levels of glutamate (Glu) and γ-aminobutyric acid (GABA) – the main excitatory and inhibitory neurotransmitters in the brain, respectively. In addition, molecules involved in prominent metabolic pathways, such as glucose (Glc) and lactate (Lac), can be accessed using high-fidelity MRS. However, given the $\sim 10^4$ lower concentration of metabolites compared to water, MRS has a much lower sensitivity compared to water-based MRI, usually leading to long acquisition times and poor spatial resolution. Increasingly higher magnetic fields provide increasingly higher signal-to-noise, thereby overcoming some of the sensitivity limitations; furthermore, higher magnetic fields also allow better spectral resolution, which can in turn increase the reliability of metabolite quantification (Mlynárik et al., 2008). However, the increased spectral bandwidths associated with higher fields also require high-power RF pulses or other alternatives (e.g. adiabatic pulses), which can then contribute to suboptimal SNR or increased SAR.

Given the abovementioned challenges with MRS, it is perhaps not surprising that functional MRS (fMRS) experiments – i.e., MRS experiments designed to probe metabolites with high temporal resolution such that their variations during a task or upon a stimulus could be measured – remain quite rare. In humans, Mangia et al. (Mangia et al., 2007; Mangia et al., 2007) and then others (Lin et al., 2012; Schaller et al., 2013; Bednařík et al., 2015, 2018; Taylor and

* Corresponding author.
E-mail address: noam.shemesh@neuro.fchampalimaud.org (N. Shemesh).

https://doi.org/10.1016/j.neuroimage.2021.117973
Received 20 November 2020; Received in revised form 11 March 2021; Accepted 12 March 2021
Available online 21 March 2021
1053-8119/© 2021 The Authors. Published by Elsevier Inc. This is an open access article under the CC BY-NC-ND license (http://creativecommons.org/licenses/by-nc-nd/4.0/)

Schaefer, 2015; Taylor and Neufeld, 2015; Betina Ip et al., 2017; Cao et al., 2017; Mekle et al., 2017; Martínez-Maestro et al., 2018; Boillat et al., 2019) harnessed the increasing availability of high field 7 T scanners to record metabolic variations upon visual stimulation, often interpreted as a result of increased oxidative metabolism upon neural activity. Koush et al. (Koush et al., 2019) were able to probe lactate variations using J-Edited fMRS at 4 T. At more conventional fields of 3 T, fMRS acquisitions were carried out following some task-based stimuli (Logothetis and Wandell, 2004; Apšvalka et al., 2015; Kühn et al., 2016; Vijayakumari et al., 2020; Volovyk and Tal, 2020), but also using acute pain stimuli (Gussew et al., 2010; Cleve et al., 2015; Archibald et al., 2020) for which associated metabolic variations are larger (Mullins, 2018). In a majority of studies, increases in Glu (1–5%) (Mullins, 2018) and Lac were evidenced in the active period. When spectral quantification was reliable enough, decreases in Glc and aspartate (Asp) levels were reported (Lin et al., 2012; Bednařík et al., 2015), as well as stimulus-dependent modulations in GABA levels (Cleve et al., 2015).

Until now, the typical fMRS paradigms involved sustained (> 5 min) sensory stimulus, to facilitate signal averaging for robust quantification of metabolites during the active/resting states and to reach a metabolic steady state. However, habituation may play an important role in such sustained stimuli and they may be less than revealing in terms of task-based neural activity. In addition, the dynamics of such slow fMRS experiments can be difficult to interpret, and, in the context of clinical applications, may not be well sustained by patients. Indeed, clinical applications in cognitive neuroscience and psychiatry research would greatly benefit from an improved fMRS temporal resolution (Stanley and Raz, 2018). Preclinical experiments, with potentially much higher magnetic fields and their associated higher spectral resolution, as well as the availability of transgenic lines and possibility of performing more invasive validation experiments, can be extremely valuable to promote a better understanding and interpretation of fMRS. The first preclinical ^{1}H-fMRS experiments were conducted in the rat (Just et al., 2013) still using sustained (> 10 min) stimuli, where increases in Glu and Lac and decreases in Glc could be observed despite the sedation. Since then, only very few other studies (Just and Sonnay, 2017; Sonnay et al., 2017; Sonnay et al., 2018; Just and Faber, 2019) have been performed in the rat and the tree shrew, generally reproducing the initial findings.

The ease of manipulating the mouse genome and the consequent vast array of transgenic lines make mouse models highly important for basic research at large. Transgenic mice offer the opportunity to perform optogenetic and chemogenetic manipulations, thereby enabling cell- or circuit specific probes of neural activity. In addition, transgenes offer the possibility of investigating many different features of disease. However, so far, only one recent study involving anesthetized mouse and functional spectroscopy has been conducted, using a relatively prolonged sensory (forepaw) stimulation (Seuwen et al., 2019). The paucity of such studies can probably be traced to difficulties associated with the very small voxel sizes required for achieving regional specificity in mouse MRS (Tkáč et al., 2004), which significantly reduce sensitivity. The difficulty is exacerbated by the need of a stable sedation (Grandjean et al., 2014), which can be more challenging in mice than in rats.

In this study, we report functional ^{1}H MRS experiments in the sedated mouse with a high temporal resolution (12 s). Rather than using a sustained stimulus, we design a block paradigm with relatively short periods of stimulation (24 s), separated by 48 s periods of rest, and followed by a recovery period that can alleviate adaptation and probe a different dynamic range which can potentially complement information arising from (water based) fMRI responses. As proof of principle, we executed a simple visual stimulation paradigm and chose the superior colliculus (SC) as the target voxel, as it receives inputs directly from the optic tract and shows very robust BOLD responses upon simple visual stimuli (e.g. Gil et al. 2021). We use a relatively common preclinical field (9.4 T) but perform the experiments using a cryoprobe, which provides a facilitating ~2.5 increase in sensitivity compared with conventional reception coils. Our observations of robust fMRS responses and the possibility to carry a dynamic analysis are stepping stones for future studies aiming to enhance the specificity of fMRI experiments in normal and diseased mice.

Material and methods

All animal experiments were preapproved by the institutional and national authorities and carried out according to European Directive 2010/63.

Animal sedation and preparation

Anesthesia in mice (N = 20 C57Bl6 females, 3-4 months old, weighting 24-26 g) was induced using ~5% isoflurane. The percentage of isoflurane was progressively decreased during animal preparation (namely, placing the animals on the animal bed and positioning the mouse using a bite bar and ear bars, medetomidine subcutaneous cannula and rectal probe insertion). The anesthesia regime was then switched to a mix of low dose isoflurane (~0.3%) in a 28% O_2/air mixture and subcutaneous medetomidine infusion (bolus: 0.4 mg/kg, constant infusion: 0.8 mg/kg/h, optimized from Grandjean et al., 2014). Temperature (maintained at 36.0 ± 0.5 °C, rectal probe) and respiration rate (120–160 resp/min, breathing pad) were monitored throughout the experiments and remained stable once the functional spectroscopy session began.

Experimental design

Scanner and coils

All data were acquired using a 9.4 T Bruker BioSpec scanner (Bruker, Karlsruhe, Germany) interfaced with an AVANCE III HD console driving a gradient system capable of producing up to 660 mT/m isotropically. The scanner runs Paravision 6.0.1 software (Bruker, Ettlingen, Germany). An 86 mm volume quadrature resonator (Bruker, Karlsruhe, Germany) was used for transmission and a 4-elements array cryoprobe (Bruker, Fallanden, Switzerland) optimized for the mouse head (c.f. also Gil et al. 2021) was used for signal reception.

Setup for delivering visual stimuli

Optic fibers delivering a flashing blue light generated by a LED (wavelength = 470 nm, intensity = 0.8 W/m^2, frequency = 4 Hz, pulse duration = 15 ms) were positioned horizontally on each side of the mouse bed at about 1 cm from each eye. The mouse vision relies on UV-sensitive photopigments and middle-wavelength photopigments with maximum sensitivity between 360 and 510 nm (Jacobs et al., 2004; Wang et al., 2010). A blue light at 470 nm was used to strongly stimulate the mouse retina. The frequency of 4 Hz was chosen since it allows for a reproducible stimulus at each repetition time and it falls into the range of frequencies (0.5–10 Hz) known to induce a robust neuronal response (Wang et al., 2010; Niranjan et al., 2016).

Stimulation paradigm

The block paradigm (BP) alternated between 48 sec without stimulation (OFF) and 24 s with visual stimulation (ON) periods. This was repeated 5 times, followed by a single OFF period. For functional MRS acquisitions, the BP was followed by a recovery (R) period of the same duration (6 min 48 s) for a total duration of 13 min 36 s per BP-R paradigm.

MRS pulse sequence adaptation

Metabolites ranging from 1 to 4 ppm were targeted and observed in this study. Therefore, to ensure that the functional signals arise from the same voxel, chemical shift displacements needed to be minimized. To this end, a LASER (Localization by Adiabatic SElective Refocusing, (Garwood and Delabarre, 2001)) sequence was implemented and

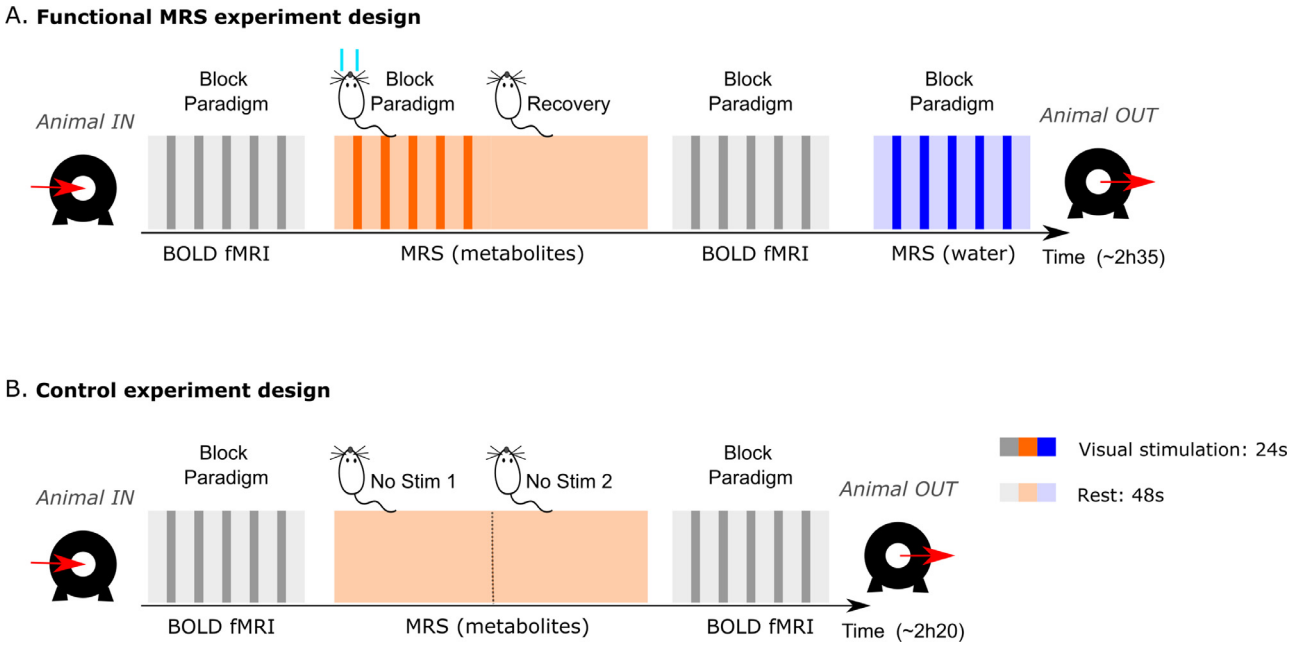

Fig. 1. Representative timelines of the functional MRS experiment **(A)** and the control experiment **(B)**. Both functional MRS and control experiments begin with a BOLD-fMRI acquisition upon visual stimulation, to verify the presence of a BOLD response in the SC in the beginning of the session (Step 1). Then, spectra are acquired in the SC during ~1 h 10 min, concatenating 5 repetitions of the ensemble Block Paradigm - Recovery (A) or No Stim 1 - No Stim 2 (B) (Step 2). Another BOLD-fMRI map is acquired to verify the presence of a BOLD response in the SC in the end of the MRS session (Step 3) for both (A) and (B). In the functional MRS experiment (A) only, functional MRS of water is then acquired in the SC.

adapted for fMRS acquisitions in this study. In particular, the phase cycling of the LASER sequence, usually counting 32 to 64 steps for a good spurious signal removal (Kingsley, 1994), was reduced to 4 steps (excitation {0 2 1 3}, refocusing {1 3 0 2), receiver {0 2 1 3}) to allow a better temporal resolution. To compensate for the suboptimal phase cycling, 4 blocks of outer volume suppression (OVS) module were added prior to signal excitation.

Timeline of experiments

Fig. 1**A** describes the principal experimental timeline for the functional experiment, which was designed to ensure robust visual activation throughout its entire duration. Below, we briefly mention each step and its role in the experimental design. Detailed parameters for pulse sequences used in each phase within the timeline are presented in the following section.

Step 1: Blood Oxygenation Level Dependent (BOLD) fMRI (~7 min). Following routine adjustments, and a well resolved anatomical image for slices and voxel positioning, this simple experiment was performed to ensure robust activation in the superior colliculus at the beginning of the experiment, following the BP.

Step 2: fMRS acquisitions (~1 h 10 min). Once a detectable BOLD-response was ascertained in the superior colliculus with a rapid analysis using PV6.0.1 routines, we proceeded with the MRS acquisitions on upfield metabolites (with the water suppression module). The BP-R was repeated 5 times.

Step 3: Repeated measurement of BOLD fMRI (~7 min). To ensure that habituation to stimulus in the superior colliculus is minimal, Step 1 was repeated, and BOLD fMRI maps were measured again.

Step 4: fMRS acquisition on the water signal (~7 min). To get the precise timing of vascular effects in the voxel of interest and attempt to account for the vascular effects on metabolite signals during post-processing, identical fMRS experiments were performed on the water signal (by turning off the water suppression module). This also verified the voxel positioning and informed about LASER-driven water BOLD responses.

Fig. 1**B** describes the control experiment. The timeline is identical to the functional experiment's timeline, except that no visual stimulation is delivered during Step 2, and Step 4 was not acquired (since vascular correction is irrelevant). For comparison with the above-mentioned BP-R paradigm, the "paradigm" of Step 2 for the control experiment was divided into two periods of 6 min 48 sec, that we termed "No Stim 1" and "No Stim 2".

Experimental parameters

Steps 1 and 3: BOLD fMRI experiments were acquired using a gradient echo EPI pulse sequence (TR/TE = 1000/12 ms), with an in-plane resolution of 0.145 × 0.145 mm^2 (axial, matrix size 110 × 96, FOV = 16 × 13.9 mm^2) and a slice thickness of 0.5 mm. The slice package (8 interleaved slices) was positioned to cover the superior colliculus and the visual cortex. The anatomical image was acquired using a T_2-weighted RARE sequence (TE/TR = 40/2000 ms, resolution: 0.075 × 0.080 × 0.400 mm^3, 15 interleaved slices).

Step 2: fMRS experiments were carried out using the adapted LASER sequence (described above) on a volume of 2.3 × 1.7 × 1.7 mm^3 voxel placed around the superior colliculus. Spectroscopic signals were collected over a bandwidth of 4000 Hz (10 ppm) with 2048 complex data points sampled (TE = 28 ms and TR = 1500 ms, total signal acquisition time = 512 ms). Hyperbolic secant (HS4) (Tannüs and Garwood, 1996) refocusing pulses (pulse duration = 2 ms, bandwidth = 10 kHz) were designed using Topspin 3.1 software (Bruker, Ettlingen, Germany). Water suppression was achieved using a CHESS (CHEmical Shift Selective saturation, (Frahm et al., 1989)) module consisting of three CHESS pulses with a bandwidth of 250 Hz, chosen for having a shorter duration than the very efficient VAPOR (variable power RF pulses with optimized relaxation delays, (Tkáč et al., 1999)). The water residual amplitude was usually lower than twice the N-acetylaspartate (NAA) amplitude. The water suppression pulses were interleaved with 4 blocks of outer volume suppression sinc10 pulses, giving a total duration for the preparation modules of 227 ms. For each BP-R paradigm (or No Stim 1 – No

Stim 2 paradigm), 544 repetitions were acquired over 13 min 36 s (× 5). The single voxel was shimmed between each block of 13 min 36 s.

Step 4: Water fMRS was acquired using the same parameters as given above, with the exception of removing the water suppression module, leading to 162 ms of preparation modules (OVS).

Data Analysis

All data in this study were analyzed using custom code written in MATLAB® (The MathWorks, Inc., Natick, Massachusetts, United States). Below we elaborate on every data analysis routine for the relevant steps.

Steps 1 and 3: BOLD-fMRI analysis he BOLD-fMRI data acquired in the beginning of the session was always analyzed "on-the-fly" with the vendor software (Paravision 6.0.1), to ensure that robust activation of superior colliculus was detected, before starting the MRS acquisitions. A more rigorous analysis with a home-made MATLAB® (MathWorks, Natick, Massachusetts, USA) routine calling SPM12 was performed later. Raw data were converted to Nifti and corrected for outliers, slice timing (taking for reference a slice comprising the superior colliculus) and motion (translation and rotation). Data was then co-registered to the respective anatomical image and normalized to the Allen Mouse Brain Atlas (Common Coordinate Framework version 3) (Lein et al., 2007) via rigid body and affine transformations, respectively. Aligned images were then isotropically smoothed using a 3D-Gaussian-kernel with a full width at half maximum (FWHM) = 0.145 mm. Individual BOLD maps were generated by fitting a GLM (high-pass filter cutoff, 90 s; motion parameters used as nuisance regressors) to the data and thresholded at a significance level of $p = 0.01$ and minimum cluster size = 4 (see **Supplementary Fig. 1** for a representative animal and for average maps). A fixed-effects group GLM analysis was then performed for each experimental step using functional data from all animals, a significance threshold of $p = 0.001$ and a minimum cluster size of 8.

Step 2: fMRS analysis.

Preprocessing

The LASER phase cycling imposed a minimum of 4 repetitions, leading to a minimum temporal resolution of 6 s. Every repetition was individually phase corrected (0 order) and drift corrected using the average spectrum as a reference via a MATLAB® home-made routine. To enhance SNR, we summed spectra over 8 consecutive repetitions (= 2 × 4 phase-cycle repetitions) providing a moving average with an effective time resolution of 12 s (apparent time resolution 6 s). The resulting spectra were then eddy-current corrected in MATLAB® using the water reference (Klose, 1990) and the water residual signal (whose amplitude was usually not greater than twice the NAA or total creatine (tCr) peak) was removed by singular value decomposition (Pijnappel et al., 1992) to ensure a flat baseline. To correct for the potential linewidth and intensity slow drifts along time (1 h 08 min of MRS acquisitions), we first concatenated the 5 blocks, normalized by their own intensity mean, to correct for potential gain variations between blocks. The data were then detrended by applying a linear linewidth correction to successive spectra, from the calculated averaged linewidth of the 3 singlets (NAA + tCr + choline compounds (tCho)), on individual blocks first (13 min 36 s) and then on the full time course (1 h 08 min). The average linewidths were computed by measuring the FWHM directly on the spectra, whose FIDs were zero filled prior to FT to improve the precision.

Time course construction

To build the time course of interest (the block paradigm followed by the recovery period, 13 min 36 s), spectra were summed along the 5 blocks (applying phase and frequency correction), yielding a final time course of 135 points with an apparent temporal resolution of 6 s, and an effective temporal resolution of 12 s. Each spectrum representative of a time-point was calculated by adding the 8 × 5 = 40 individual repetitions, which allowed a robust metabolite quantification for individual animals.

Correction for BOLD-induced line narrowing

Positive BOLD responses in active areas can induce an increase in T_2/T_2^* and therefore a linewidth narrowing, which in turn can bias the signal quantification (Zhu and Chen, 2001).

Under the hypothesis that BOLD effects would impart similar dynamics on both water and metabolite signals, we used the water fMRS measurements as a reference for BOLD-induced time courses, taking advantage of its high SNR. The linewidth and amplitude of the water signals were computed for the water fMRS experiments to spot the empirical timeline of the BOLD events (underlined in light grey on **Fig. 2B/2C**). As an example, we corrected for the T_2/T_2^* effect on water by applying a line broadening of 0.4 Hz during the identified BOLD events. Temporal fluctuations of water linewidth due to BOLD activation were thus effectively removed (**Fig. 2C**, right panel).

The same approach was applied to the metabolites time courses (**Fig. 3**) (Mangia et al., 2007). We computed the average linewidth and amplitude along the BP-R paradigm for the singlets of the upfield spectrum (NAA + tCr + tCho, **Fig. 3B/3C**). We then applied a line broadening of 0.5 Hz during the predefined BOLD events. Quantitatively, this correction matches, at best, the average linewidth during the BP and the average linewidth during the recovery period (**Fig. 3C**). However, to account for cross-subject differences, we chose corrections individually for each animal (**Fig. 3A**) by computing the difference between the averaged spectra of the BP and the Recovery periods, and applying a line broadening during the vascular events (between 0.5 and 0.7 Hz) that minimized the residuals of the 3 main singlets (**Supplementary Fig. 2A**). Three (out of the 10) animals scanned for the functional experiment were detected as outliers: for these animals the nulling of the singlets' residuals required a line broadening > 1 Hz, corresponding to a linewidth drift independent of a BOLD effect. In the control group, two outliers were detected (**Supplementary Fig. 2B**). To make both the functional and the control experiment comparable in number, we removed these outliers and one more control mouse which had the poorest spectral quality, leaving N = 7 mice in each group.

Time course quantification

The BOLD-corrected fMRS spectra were quantified using LCModel (Provencher, 1993). A home-made routine based on the density matrix formalism (Mulkern and Bowers, 1994) generated a basis set of 21 metabolites (Acetate, Alanine, Ascorbate, Arpartate, Choline, Creatine, GABA, Glucose, Glutamine, Glutamate, Glycine, Glycerophosphocholine, Gluthatione, Myo-inositol, Scyllo-inositol, Lactate, N-Acetylaspartate, N-Actetylaspartateglutamate, Phosphocholine, Phosphocreatine, Taurine), using the chemical shift database in Govindaraju et al. (2000). An empirical macromolecule baseline was included in the basis set for a more robust spectral quantification (Giapitzakis et al., 2019). Macromolecule spectra were acquired during previous experiments in the same voxel by implementing a double inversion recovery module prior to the LASER localization block (first inversion time = 2200 ms, second inversion time = 700 ms, chosen for the resulting good apparent metabolic nulling, close to (Lopez-kolkovsky et al., 2016)). All other parameters were identical to the MRS acquisitions (Step 2) except the TR that had to be prolonged to 4000 ms to incorporate the double inversion module.

Spectra were fitted between 0.4 and 4.2 ppm. To obtain the normalized time course for every metabolite, the absolute concentration (as fitted by LCModel) was normalized by the corresponding average concentration during the recovery period (or during "No Stim 2" period for the control experiment) for every time point.

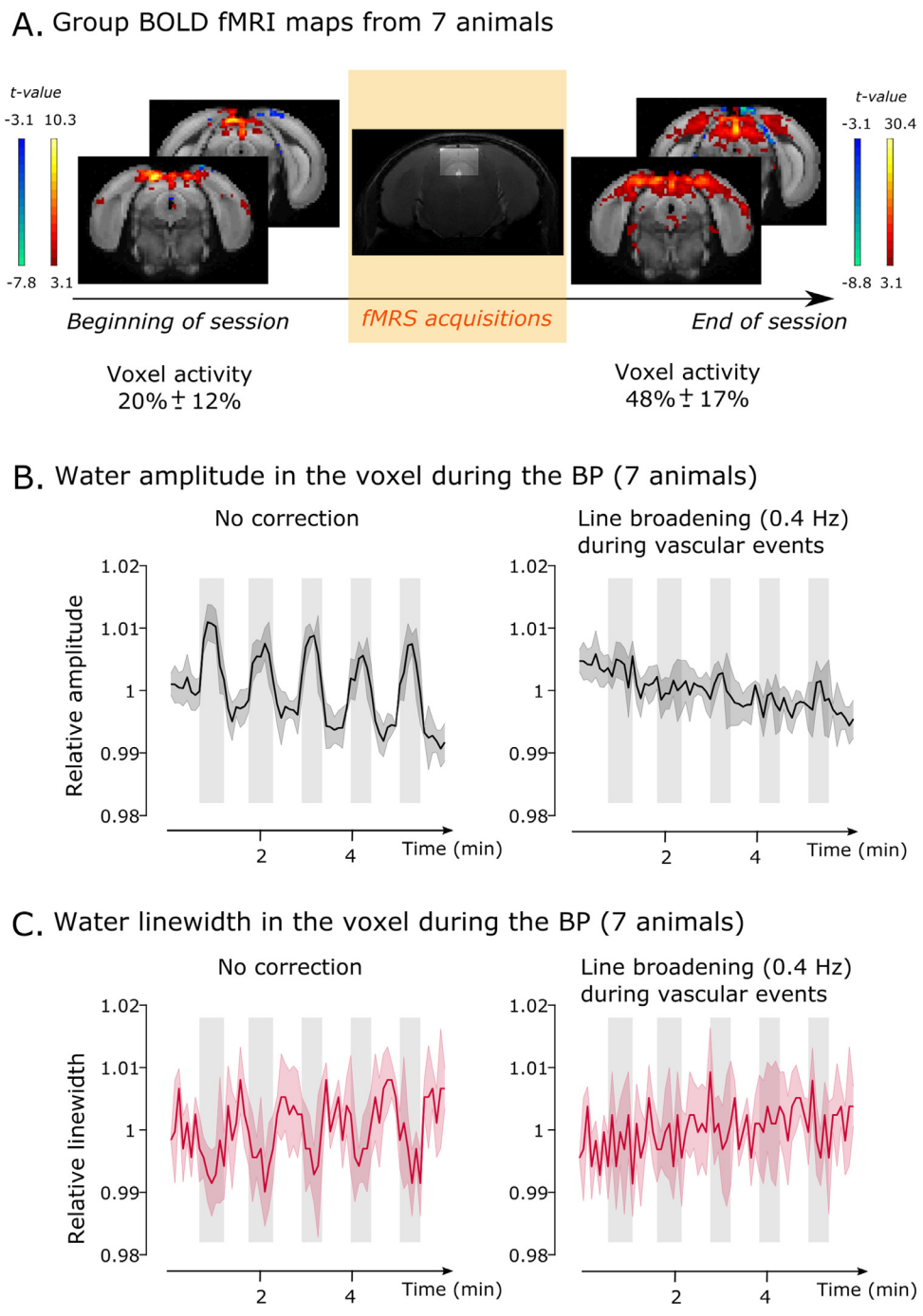

Fig. 2. BOLD responses upon visual stimulation delivered in a block paradigm (BP). **(A)** Animal-averaged BOLD fMRI maps aligned on the Allen Reference Mouse Brain Atlas, acquired in the beginning and in the end of experiments, with a significance threshold of $p = 0.001$. **(B)** Animal-averaged time course of the water peak amplitude acquired in the voxel around superior colliculus during the block paradigm (Step 4) without any correction, used to define the BOLD events, enhanced in light grey (left). A line broadening of 0.4 Hz is applied during the defined BOLD events to exemplify the effect of such a correction (right). **(C)** Animal-averaged time course of the water linewidth acquired in the voxel around superior colliculus during the block paradigm (Step 4) without any correction (left) or with a line broadening of 0.4 Hz applied during the predefined BOLD events (right). The shadows represent the standard deviations.

Difference spectra

This analysis aimed at comparing the so-called "active period" (6 min 48 s of the BP) and the recovery period. We averaged spectra (with phase and frequency correction) from all time-points from the BOLD-corrected BP and subtracted the corresponding average spectrum from the recovery period. The same analysis was performed for the control experiment between the "No Stim 1" and "No Stim 2" periods.

Results

Robust activation of the superior colliculus in the fMRS experiment

Group BOLD-fMRI maps acquired prior to the fMRS experiments and after their completion are shown in **Fig. 2A** (full maps are found in **Supplementary Fig. 1**, alongside with a representative animal EPI map). Maps are aligned to the Allen Reference Mouse Brain Atlas (Lein et al., 2007) for a better visualization of activated areas. Robust BOLD responses were observed in both instances, with similar, although not identical, spatial patterns. The averaged voxel activity is 20 ± 12 % in the beginning of the session, and 48 ± 17 % in the end of the session (a voxel was considered active on an individual animal if its t-value was larger than 2.34). The weaker activity in the beginning of the session likely occurs because the isoflurane induction had not fully washed out yet. However, positive activation was always robustly observed in the superior colliculus, and in other visual areas such as the primary visual cortex and the lateral geniculate nucleus.

Clear BOLD responses were observed in the time courses of the functional MRS acquisitions on water (**Fig. 2B**), suggesting adequate placement of the volume of interest. The superior colliculus contribution to the VOI reaches 50 ± 4 %, as derived from a manual segmentation of the superior colliculus on the 7 animals included in the functional ex-

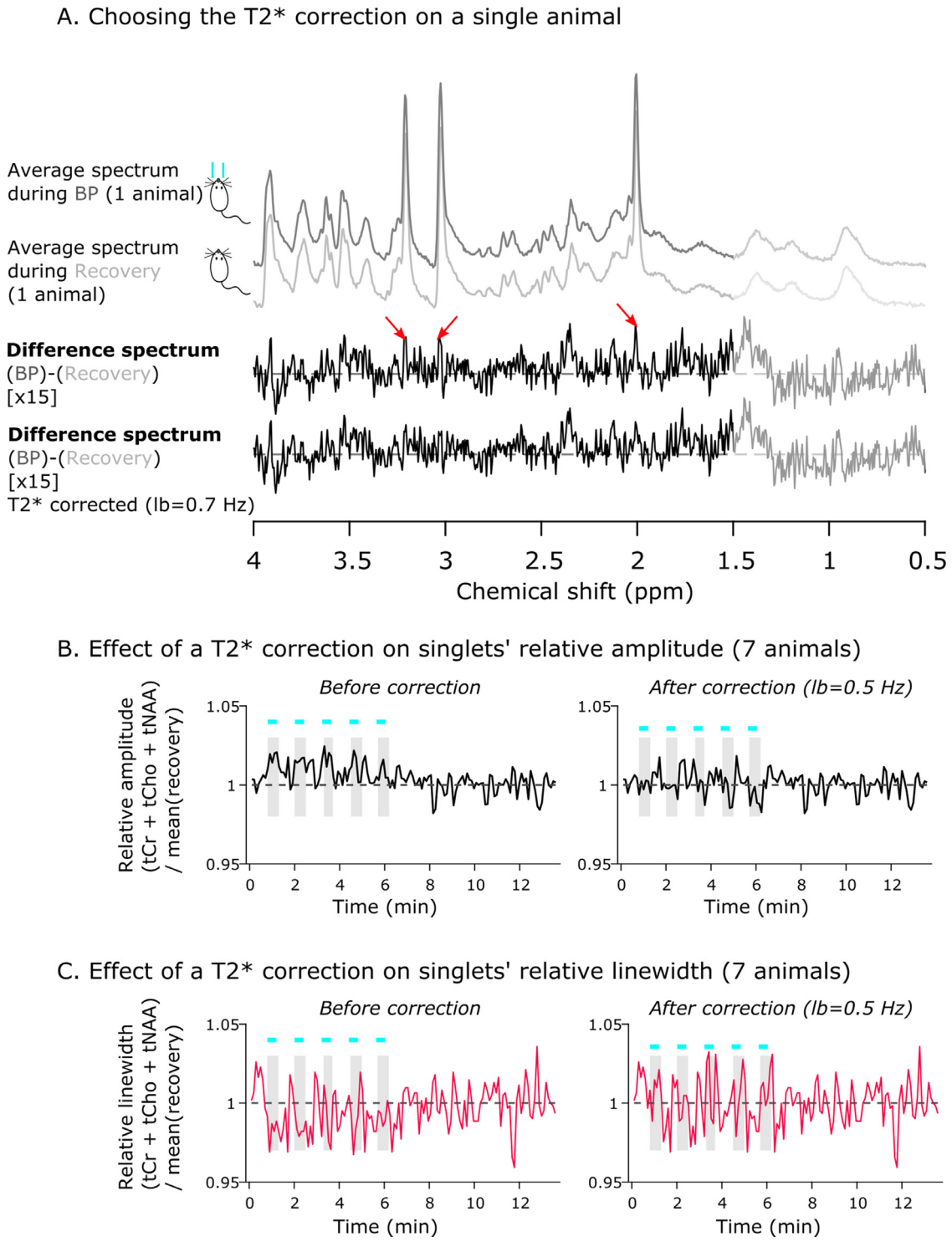

Fig. 3. Correcting BOLD effects on metabolite signals. **(A)** Example of T_2^* correction on a representative animal. A difference spectrum is generated from the difference between the average spectrum during the Block Paradigm (BP) (dark gray) and the Recovery period (light gray). The T_2^* correction was applied during the predefined BOLD events. The line broadening was chosen to visually minimize the residuals of NAA, tCr and tCho. The region below 1.5 ppm is very variable, and should not be taken into account for interpretation. **(B)** Average amplitude of the 3 singlets (NAA+tCr+tCho) computed from the time course of the all-animal-averaged spectra. The correction consists in a line broadening of 0.5 Hz applied during the predefined BOLD events (light gray). The light blue horizontal bars represent the periods of visual stimulation. **(C)** Average linewidth of the 3 singlets (NAA+tCr+tCho) computed from the time course of the all-animal-averaged spectra. The correction consists in a line broadening of 0.5 Hz applied during the predefined BOLD events (light gray). The correction was chosen to obtain the same average linewidth during the block paradigm and the recovery period. The light blue horizontal bars represent the periods of visual stimulation (For interpretation of the references to color in this figure legend, the reader is referred to the web version of this article.).

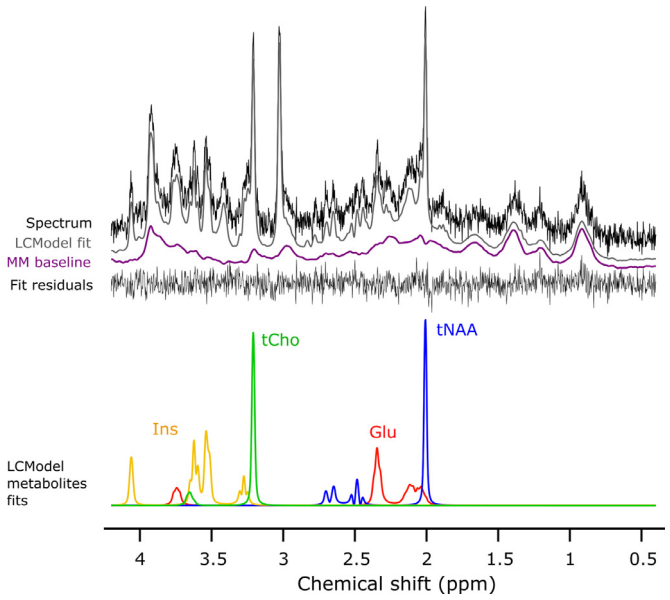

Fig. 4. Representative spectrum of one time point (chosen from the Recovery period) in one animal and the corresponding LCModel fit. The basis used for the linear combination incorporated 21 metabolites. The corresponding fit is shown for NAA, tCho (GPC + PCho + Cho), Glu, Ins.

periment group. The rest of the VOI is mostly composed of subcortical structures (notably periaqueductal gray) and small contributions from other cortical structures. Only the very rostral part of the voxel might contain the sagittal sinus.

fMRS experiments - spectral quality

The SNR of a spectrum at one time point (representative spectrum, Fig. 4) was 27 ± 3 for the NAA resonance at 2.0 ppm (corresponding average linewidth = 13.2 ± 1.8 Hz), 29 ± 3 for the tCr resonance at 3 ppm (corresponding average linewidth = 12.9 ± 1.1 Hz) and 28 ± 3 for the tCho resonance at 3.2 ppm (corresponding average linewidth = 13.0 ± 1.5 Hz). The SNR was defined as the ratio of the peak height to the standard deviation of the noise. The values for SNR and linewidth are given by mean ± standard deviation. The chemical shift displacement between NAA (at 2 ppm) and tCr (at 3 ppm) equals 4% (0.09 mm in the axial plan and 0.07 mm in the coronal and sagittal plans). The individual CRLB (Cramer-Rao Lower Bounds) were smaller than 5% on individual time points for NAA, tCr, tCho, myo-inositol (Ins), Glu, taurine (Tau) and macromolecules. The baseline fitted by LCModel was generally flat, suggesting a good quality of localization, water suppression and macromolecular fit.

The difference spectrum reveals metabolic differences between active and recovery periods

To facilitate comparisons with prior literature, we first considered the entire block paradigm as an "active" period, in contrast with the recovery period, and compared it with the recovery period. Subtraction spectra for the control experiment – namely the subtraction of the fMRS spectrum arising from the No Stim 1 and No Stim 2 periods averaging over all animals – are presented in Fig. 5**A** while the subtraction spectra arising from the Active and Recovery periods (again, averaged over all animals and corrected for vascular events as described in the Methods) are shown in Fig. 5**B**. The difference spectrum of the control experiment reveals non-vascular residuals for NAA, tCr and tCho, that can also be observed in the difference spectrum of the functional experiment. The principal disparity between the two difference spectra is the robust residual at 2.3 ppm that corresponds most likely to glutamate resonances. The region below 1.5 ppm was characterized by a large variability between animals (**Supplementary Fig. 2**).

To compare the active period with the recovery period, we also computed the concentration distributions of metabolites for the BP and the recovery period, each value corresponding to 1 time point in 1 animal. Histograms for Glu, Ins, tCho and Glu are shown in Fig. 6**B** (Tau and tCr histograms are plotted in **Supplementary Fig. 3**). Similarly, we compared No Stim 1 and No Stim 2 (Fig. 6**C**). A consistent increase of glutamate during the block paradigm can be seen via a clear shift towards higher concentrations in the first part of the functional experiment, while there is no shift in the control distribution. Otherwise, a slight drift is observed for NAA (and Tau) in both the functional and control experiments. tCr exhibits a stronger drift in the control experiment than in the functional experiment.

Dynamic time courses of reliable metabolites (CRLB ≤ 5%), temporal resolution 12 s

The average time courses of NAA, tCr, tCho, Glu, Ins and Tau were computed from the individual time courses of the functional and control experiments (Fig. 6**A, Supplementary Fig. 3**). To account for the different noise levels of the different metabolites, we compared the metabolic variation with the coefficient of variation (CoV) defined during the recovery period (respectively the "No Stim 2" period) and represented it on the time courses by a dotted gray line. Glutamate is progressively upregulated during the visual stimulation. As for the inference of a more dynamic information, there does not seem to be an increase in glutamate locked to the short periods of stimuli (24 s, highlighted in light blue on Fig. 6**A**), but the noise level prevents drawing more quantitative conclusions. The other metabolites present similar time courses between the functional and the control experiment, except for tCr, whose drift is stronger in the control experiment (**Supplementary Fig. 3**).

Despite their much higher CRLB, time courses and distributions of N-acetylaspartateglutamate (NAAG) (mean CRLB = 10), phosphocreatine (PCr) (mean CRLB = 7) and creatine (Cr) (mean CRLB = 11) are displayed in **Supplementary Fig. 4**, for their (qualitative) different patterns between the functional and the control experiment. In particular, we notice a downregulation of NAAG during the block paradigm and an upregulation of Cr, and slight downregulation of PCr.

Generalized Linear Model (GLM) regression on time courses

To derive a more quantitative analysis regarding the signal dynamics, enabled by the relatively high temporal resolution in this study, we ran a simple GLM regression on the average time courses of NAA, tCr, tCho, Glu, Ins and Tau. The GLM incorporated the block paradigm, the active/recovery design to assess for slow metabolic response, and a linear drift (Fig. 7**C**). After a multiple comparison correction, NAA varied significantly with the individual 24 s periods of stimulation in the block paradigm during the functional experiment, while Glutamate varied significantly with the active/recovery design, but not with the individual 24 s stimulation periods. During the control experiment, NAA, tCr, tCho exhibited a significant drift (**Table 1**).

With a finite impulse response approach (13 blocks of 1 min), we also estimated the "metabolic response function" (MRF) of the different metabolites (Fig. 7**A**). Glutamate MRF ramps up until the second period of stimulation (~3 min), stays high until the last period of stimulation (ending at 6 min) and decreases in the end of the BP. In comparison, the other metabolites do not exhibit MRF with a specific pattern.

Discussion

In this work, we aimed to develop a fMRS paradigm in mice with a high temporal resolution. The main motivation for extending fMRS

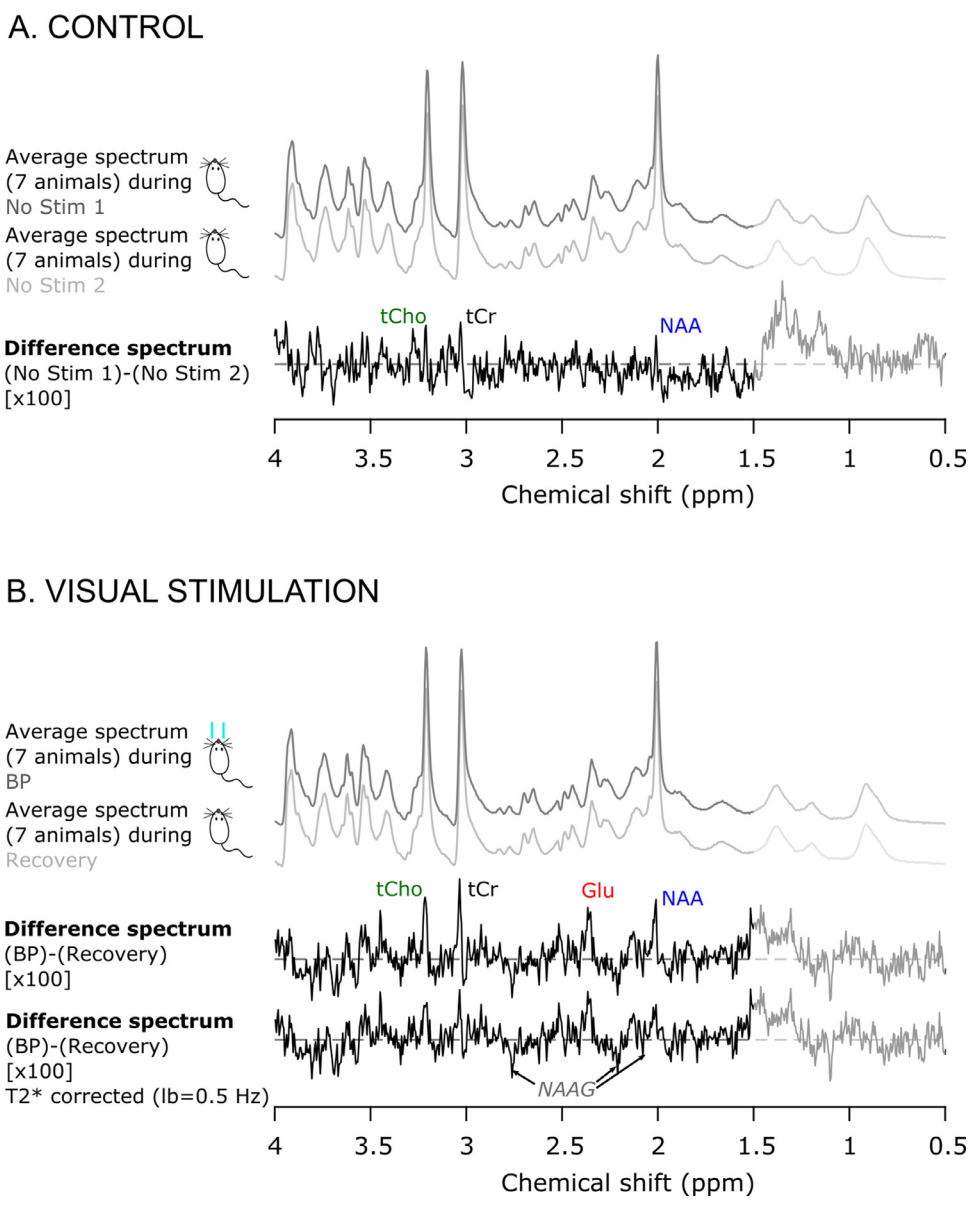

Fig. 5. Spectral differences between the different experimental blocks. **(A)** Difference spectrum between the spectrum of the No Stim 1 period (dark grey) and the No Stim 2 period (light grey), averaged over all animals. **(B)** Difference spectrum between the spectrum of the Block Paradigm (dark grey) and the Recovery period (light grey), averaged over all animals. For visualization purposes, a line broadening of 4 Hz has been applied on all difference spectra. Note that the region below 1.5 ppm in all spectra is very variable and deemed untrustworthy.

Table 1
p-values for the GLM analysis achieved on metabolites time courses for both the functional and the control experiment, whose regressors are described in Fig. 7C ("Drift", lower row; "Block Paradigm", middle row; "Active/Recovery", upper row). *p*-values < 0.05 are highlighted in **bold**. When applying a Bonferroni correction for multiple comparison (6 metabolites), the *p*-values becoming > 0.05 are highlighted in *italic*.

	FUNCTIONAL			**CONTROL**		
	Drift	Block Paradigm	Active/Recovery	Drift	Block Paradigm	Active/Recovery
NAA	*0.114*	**0.018**	0.081	**6.42E-05**	0.131	0.24
tCr	0.116	*0.09*	0.567	**0.002**	0.817	0.718
tCho	0.756	0.133	0.552	**0.030**	0.14	0.548
Glu	0.812	0.512	**0.025**	*0.271*	0.053	0.834
Ins	0.467	0.222	0.733	0.35	0.989	0.539
Tau	0.122	0.629	0.67	0.206	*0.15*	0.371

experiments to mice is due to the prominence of genetic mouse models both in basic research (e.g., through enhanced cellular specificity) and in genetic models of diseases (e.g., through specific manipulations of genes inducing disease phenotypes). Rodent models in general, and mouse models in particular, are useful for post-hoc invasive procedures, as well as the predominance of preclinical high field MRI scanners with high-performing probes can thus bridge the mouse-to-human gap and assist in explaining the nature of observed modulations. In the mouse, it is for example possible to use a pharmacological stimulus directed towards a specific neurotransmitter receptor, such as bicuculline, a GABA-A receptor antagonist, to specifically assess transient changes in neurotransmitter and metabolites levels (Seuwen et al., 2015). Optogenet-

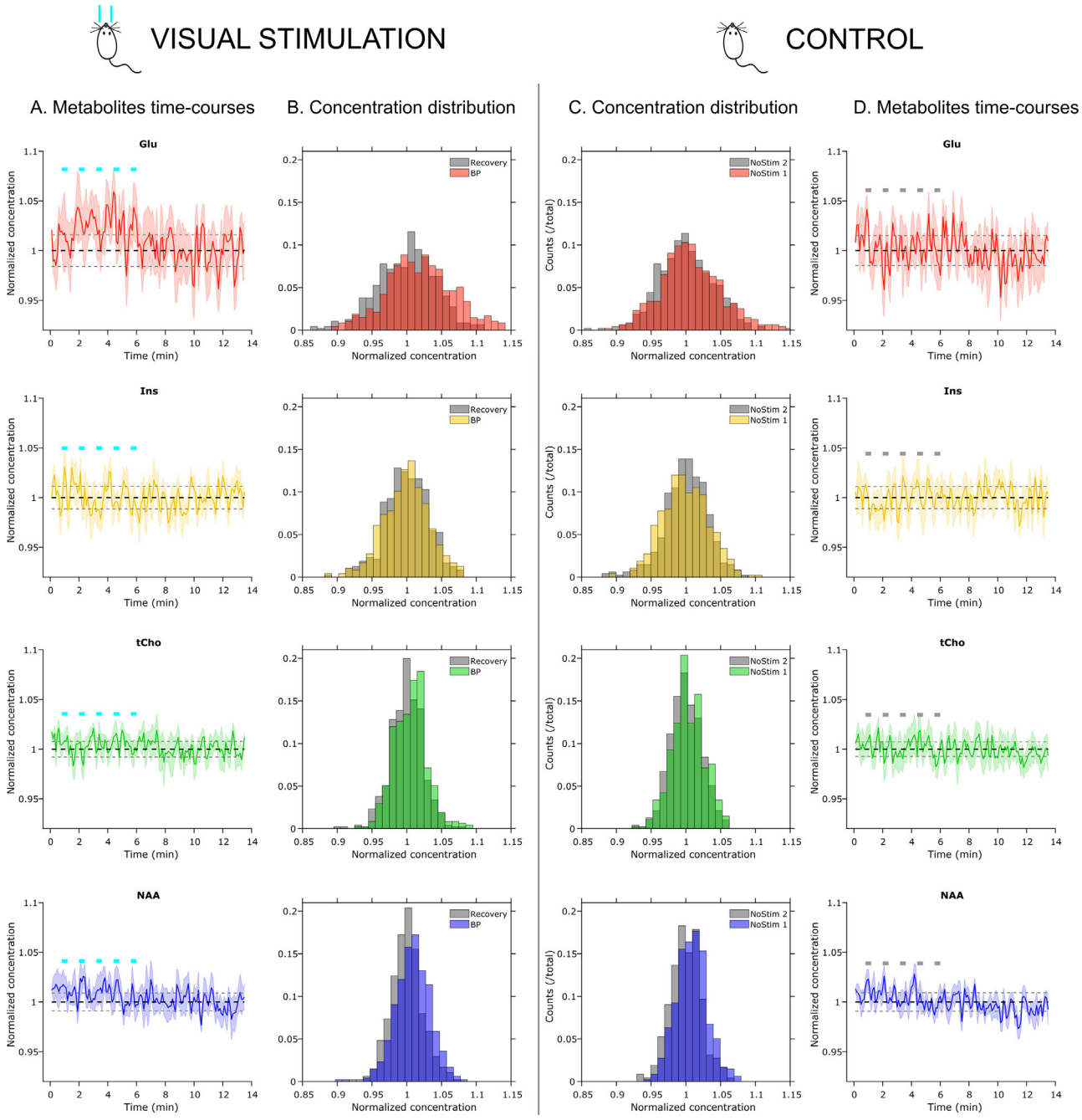

Fig. 6. Time course analysis. **(A)** Relative concentrations time courses for Glu (red), Ins (yellow), tCho (green) and NAA (blue) during the Block Paradigm (BP) and the Recovery period, normalized by their mean during the Recovery period. The dotted gray line represents the coefficient of variation of the data calculated from the standard deviation and the mean during the Recovery period. The light blue horizontal bars represent the periods of visual stimulation. **(B)** Relative concentrations distributions for Glu (red), Ins (yellow), tCho (green) and tNAA (blue) during the Block Paradigm (BP) and the Recovery period, normalized by their mean during the Recovery period. **(C)** Equivalent concentration distributions for the control group (No Stim 1 vs No Stim 2, normalised by their mean during No Stim 2). **(D)** Equivalent concentration time-courses for the control group in (A), normalised by their mean during No Stim 2. The light grey horizontal bars are for timing visualisation. (For interpretation of the references to color in this figure legend, the reader is referred to the web version of this article.).

ics lines expressing channel rhodopsin specifically in glutamatergic or GABAergic neurons (Zhao et al., 2011) could help disentangling the role of excitatory and inhibitory neurons in signal change (n.b. a recent study combining optogenetics and fMRS in rats (Just and Faber, 2019)). Moreover, the well-established pharmacology available in rodents and the chemical genetic lines (such as DREADDs, (Roth, 2016)) are preclinical tools allowing, among others, manipulations of diverse cell metabolic pathways or of synaptic release, and therefore have the potential to unravel the nature of the fMRS modulation. The increasing number of mouse models of psychiatric and neurodegenerative diseases reinforces the interest for translational approaches with fMRS. Furthermore, unlike nearly all previous fMRS experiments in rodents which harnessed sustained stimulation, the short-stimuli paradigm here introduced could be a first step towards a better comparison with the more conventional fMRI experiments. The paradigm used here could also contribute to understanding of fMRS signals observed in humans and to interpreting the ensuing metabolic variations. For example, several studies interpret variations of Glu, but more particularly GABA, as reporters of excitation

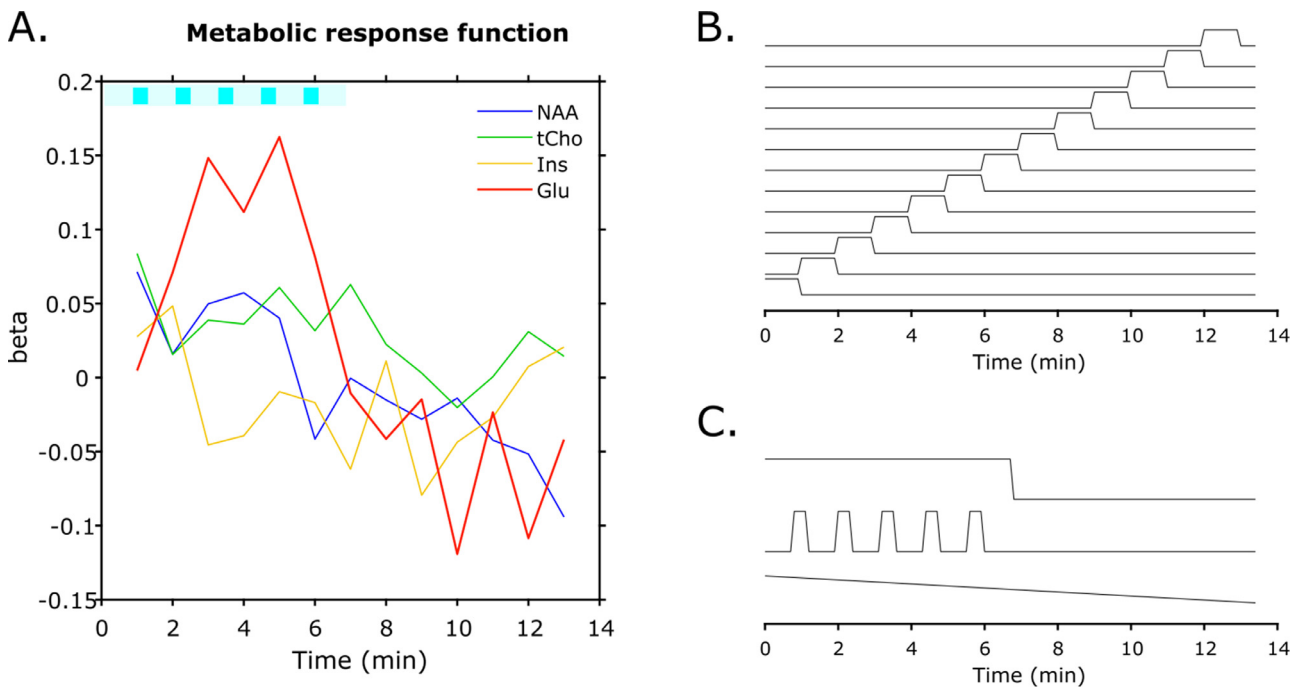

Fig. 7. General Linear Model approach. **(A)** Metabolic response function estimated for Glu, NAA, tCho and Ins with the Finite Impulse Response approach. A light blue bar represents the Block Paradigm timing, the 24 s stimulation periods are highlighted in cyan. **(B)** The regressor matrix for (A) contains 13 regressors of shifted one minute "on" periods. **(C)** The regressor matrix corresponding to the GLM analysis whose results are shown in Table 1 contains 3 regressors: a linear drift (lower row), the block paradigm design (middle row) and active/recovery design (upper row).

or inhibition mechanisms, respectively (Cleve et al., 2015; Mekle et al., 2017; Stanley and Raz, 2018; Bezalel et al., 2019; Boillat et al., 2019), potentially making fMRS attractive for psychiatric diseases, where an altered excitation/inhibition balance is often pointed out (Marín, 2012).

Our findings of robust increase of glutamate during the block paradigm is in good agreement with previous fMRS literature, both in humans and in rodents. As the main excitatory neurotransmitter and most abundant amino acid in the adult mammalian brain, glutamate is involved in numerous metabolic pathways (Danbolt, 2001; Magistretti and Allaman, 2015). It is mostly present in the cytoplasm, but is also densely located in synaptic vesicles, in mitochondria and in the synaptic cleft. Commonly associated to neurons in the CNS, glutamate is also uptaken by astrocytes, where it is immediately converted to Glutamine via the glutamate-glutamine cycle. Since the different glutamate pools might have different relaxation and diffusion properties, glutamate production, but also compartmentalization, could contribute to fMRS signals in general. Therefore, our fMRS experiments measuring relative concentrations cannot clearly resolve the origin of the observed glutamate upregulation in our experiment. A general linear model analysis is widely used in fMRI to account for the different sources of signal variation, and was here used to at least assess the dynamics (rather than the origin) of the signal. Indeed, fMRS approaches could benefit from GLM for comparison with dynamic paradigms in human studies. It is interesting to note in this context that we find that the modulation is not stimulation-locked (Table 1 and **Fig. 7**), as perhaps could be expected for neurotransmission events with fast dynamics; rather, the slow increases in Glu more likely reflect some sort of metabolic adaptation, e.g., agreeing with Bednařík et al. (2015) where 20 s time courses were reported. The progressive increase of glutamate during the block paradigm could also reflect an increased oxidative metabolism, in response to the stimulation, as hypothesized in Bednařík et al. (2015). Experiments based on this experimental setup could help address the origin of the glutamate modulation. From a protocol perspective, varying the paradigm with different inter-stimulus intervals and stimuli duration (as in (Volovyk and Tal, 2020)) can bring more dynamic insights. From the MR perspective, varying the echo time to probe the glutamate T_2-compartmentalisation, or multiparametric MRS approaches (Kirov and Tal, 2020) could provide information about the glutamate pool contributing to the modulation. Another approach consists in weighting spectra with diffusion gradients to obtain morphological insights about the glutamate pools. On preclinical setups, the maximal gradient strength is usually high enough to reach high diffusion-weightings at relatively short echo times and obtain information about the restricted compartments (Palombo et al., 2017). For example, if the increase in glutamate is due to an increased oxidative metabolism, we expect the mitochondria to produce more glutamate and therefore we might measure an increase of the Glu sphere fraction, with a low diffusivity in the spheres correlating with the high mitochondrial viscosity. If it rather arises from an enhanced synaptic release in the cleft, it is possible that the sphere fraction, characterizing the very restricted diffusion, increases as well. But we might then measure a higher associated diffusivity in the "spheres" than in the cytosol, since the extracellular space, despite being crowded in the synaptic cleft, seems to exhibit a faster diffusion (Vincent et al., 2021). Although many unknowns render this discussion speculative, diffusion-weighted MRS has the potential to help unravel the nature of the glutamate modulation. The main challenge for this approach resides in the limited SNR available at high diffusion-weightings. Finally, from a physiological perspective, the mouse is a good platform for multitude pharmacological and genetic tools. A first relatively straight-forward and controlled pharmacological experiment would be to inject a GABA-A agonist, such as muscimol, to modulate the local SC neuronal activity, and observe how it affects the metabolic response upon visual stimulation. The SC being afferent to the skull in the mouse, the procedure would be minimally invasive, and it would even be possible now to use a paramagnetic version of the muscimol to monitor the affected area during the scan (Bricault et al., 2020).

We also observed more subtle decreases in NAAG levels in this study (**Fig. 5B**). NAAG is a neuropeptide particularly concentrated in the inhibitory layers of the SC (Tsai et al., 1993), that may serve as an antagonist and a precursor of glutamate (Robinson et al., 1987). Therefore,

mutual variations in NAAG and glutamate in the activated region could be expected.

Our relatively good spectral resolution disentangles PCr from Cr (with the 4 ppm resonance). Several functional ^{31}P MRS studies reported an increase in the PCr signal during visual stimulation in the human brain. In a recent study (Hendriks et al., 2019), the authors reported an increase in PCr amplitude, but a decrease in linewidth during periods of stimulation, and therefore described it as a BOLD effect. In van de Bank et al. (2018), an increase in the PCr amplitude was reported but no linewidth modulation during stimulation was noted, thereby suggesting that PCr is upregulated during stimulation independently of BOLD effects. However, PCr is a source of phosphate ions for ATP production, and interestingly we observed a downregulation of PCr (and a consistent upregulation of Cr), especially in the beginning of the block paradigm. The phosphate moiety of PCr could be used to regenerate ATP, as a primary metabolic response. This result is consistent with a recent study in the sedated tree shrew at 14.1 T (Sonnay et al., 2018) and with the study of (Seuwen et al., 2015), using bicuculline, where the seizure onset was associated with an increased energy demand and reports a very significant decrease in phosphocreatine. Since the sensory stimulus we delivered does not induce seizures but rather increases in energy demand, a lower effect size of PCr/Cr levels can be expected and was indeed observed. The ability to monitor PCr/Cr levels using fMRS may be useful for future studies aiming at mapping relevant diseases in the future.

Several prior fMRS studies reported increases in lactate levels during the activation period (Prichard et al., 1991; Mangia et al., 2007; Gussew et al., 2010; Lin et al., 2012; Schaller et al., 2013; Just et al., 2013; Bednařík et al., 2015, 2018; Just and Sonnay, 2017; Mekle et al., 2017; Boillat et al., 2019; Koush et al., 2019) and associated with the activity of the astrocyte-neuron (particularly excitatory) lactate shuttle. In this study, however, changes in Lac were not observed. This may be due to the spectral instability in the lipid area in our study that arises from the reduced LASER sequence phase-cycling. In a voxel relatively close to the skull, this instability can prevent a reliable detection of lactate levels. Furthermore, the basal lactate levels were very low in the VOI: even in high-quality average spectra, we were never able to clearly observe the lactate doublet at 1.3 ppm. Another factor may be the anesthesia: isoflurane is known to increase the basal lactate concentration. In our study, medetomidine was used in combination with low levels of isoflurane thereby potentially even further reducing basal lactate concentration (Boretius et al., 2013). A recent study using medetomidine in rats (unlike most other studies that used alpha-chloralose) also did not report changes in lactate during sensory or optogenetic stimulation (Just and Faber, 2019). In addition, most of the studies reporting a lactate increase during an active period delivered a sustained stimulus (> 2 min) or a prolonged task. In our work, the visual stimulus was delivered through a block paradigm with repeated short periods of visual stimulation (24 s), and not through a sustained or very long stimulus, where lactate might accumulate in the cell before being cleared out. Finally, the superior colliculus is a subcortical brain area while previous studies measured fMRS responses in cortical regions. In a recent rat fMRS study an increase of lactate levels in the somatosensory cortex was reported, but when the responses were measured in the subcortical thalamus area, similar variations were not reported (Just and Sonnay, 2017). It may be that in subcortical areas, Lac production is less prominent, although this requires further studies to be concluded.

From a methodological perspective, we note our choice of the LASER sequence for the acquisition, which minimizes the chemical shift error displacement. More importantly, its CPMG-like train of 180º pulses renders the sequence relatively insensitive to the BOLD effect coming from neighboring big vessels, such as the sagittal and transverse sinuses. The phase variations occurring close to these large vessels are refocused by spin-echo like sequences: water and metabolites are typically considered as resonating in the static dephasing regime (Yablonskiy and Haacke, 1994). Coupled to the high field that weights more the contribution of the extravascular space, the signal variation observed on water (**Fig. 2B**) therefore likely reflects more of an extravascular BOLD effect from neighboring small vessels. Metabolites have a much lower diffusion than water, so it is an interesting question whether the metabolites are subject to the same diffusion regime as water. It is likely that even a LASER sequence does not completely refocus dephasing effects arising from BOLD, despite that the metabolite diffusion coefficient is much lower than water's diffusion coefficient. Hence, it is likely that a small correction may still need to be applied. However, more studies taking into account models of susceptibility (Buxton, 2013), diffusion-driven attenuation and cross terms are required to assess this issue more quantitatively.

Our work also points to the importance of a control experiment characterizing the time course of metabolites during long periods, as signal drifts may "masquerade" as activation (**Fig. 6, Supplementary Figs. 3 and 4**). Despite the shim drift correction, there might also be a metabolic drift, since anesthetics are affecting metabolism and measured metabolites concentrations (Boretius et al., 2013). It appears that the metabolic drift is more pronounced in the control experiment than in the functional experiment: it is possible that the activity induced by the visual stimulus helps maintain the metabolic homeostasis under sedation.

The LCModel quantifies metabolites using the NMR signature area of each metabolite, that accounts for the linewidth shape, and therefore should be insensitive to T_2^* variation. However, some simple simulations (applying a variable line broadening on one spectrum) show that the concentration of some metabolites given by LCModel is affected by a linewidth difference of 0.5 Hz (up to 1-2%), and even more intensely with noisy spectra (data not shown). Therefore, the correction for T_2^* effect (**Figs. 2 and 3**) associated to the neurovascular coupling is a crucial postprocessing step, but the method is empirical and thus far from ideal. The line broadening in this study was applied to correct for T_2^* effect on NAA, tCho and tCr together; however, the linewidth of these metabolites might change slightly differently depending on their compartmentation and their proximity to vessels or at different times in the experiment. Other non-vascular mechanisms could also induce dynamic T_2 variations (relative change in compartmentation for example), suggesting that more robust T_2^* correction methods should be developed.

Finally, limitations associated to single voxel MRS and sedated animals also affect this study. The superior colliculus has a very heterogeneous structure, composed of 7 layers, with different types of neurons (May, 2006). The visual input arrives in the superficial layers of the SC (in the 3rd layer), and provokes an excitation followed by an inhibition from neurons in the 2nd layer. The volume of interest is placed around the complete structure (i.e. the 7 layers), and our measurements necessarily suffer from partial volume effect and heterogenous neuronal response. The 1H-MRS methodology provides a lot of information but is also prone to error during quantification: the spectral region is crowded, and resonances from metabolites and macromolecules overlap. Although the use of a high magnetic field partly resolves this confound, metabolites still overlap with macromolecules at short echo time. The inclusion of a macromolecule spectrum in the basis set improves the robustness of the quantification, but as all empirical method, it is prone to imperfections. Metabolites residuals in the baseline could slightly impact their quantification, notably for tCr and NAA here. The use of sedation is also a confounding factor that might modulate metabolism and neurotransmission. Medetomidine is an α_2-adrenergic agonist, however the density of α_2-adrenergic receptors is quite low in the SC (Wang et al., 1996), so the effect should be mostly indirect. Isoflurane binds to many receptors and its action mechanism is not clearly established, however we use it at very low dose (0.3%) to stabilize the medetomidine sedation, moderating its impact. Moreover, the study of Seuwen et al. (2019) reported a glutamate increase upon forepaw stimulation and isoflurane anesthesia (at 1.5%) specifically in the contralateral somatosensory cortex, limiting the impact of isoflurane on specific fMRS responses.

Conclusion

A short-stimuli paradigm coupled to functional magnetic resonance spectroscopy experiment with high temporal resolution (12 s) was successfully developed and applied in the sedated mouse. Consistent glutamate increases were measured in the superior colliculus upon visual stimulation, delivered with a block paradigm that is typically used for BOLD-fMRI. The effective time resolution (12 s) and our paradigm design (discontinuous stimulation) enabled a dynamic analysis with a GLM commonly used in fMRI analyses. Under our experimental conditions, the glutamate modulation measured by MRS is not locked to the stimulus and is likely partially independent from the neurotransmission events. Pushing the temporal resolution in clinical and preclinical fMRS studies and apply analysis tools already available in the field of functional imaging can broaden the range of applicable stimuli and increase the interest and impact of fMRS studies. This study opens up the possibilities for the exploration and application of fMRS in the mouse, the richest mammalian animal model in terms of genetic lines and pharmacological tools.

Credit author statements

NS conceived of the project, procured funding, designed research, oversaw research and wrote the paper. CL designed research, performed research, analyzed data, contributed new analytic tools, and wrote the paper. FF assisted with performing research and data analysis. All authors proofread the paper.

Data and code availability statement

All authors certify that the data and code described in this manuscript will be made available upon reasonable request.

Acknowledgments

This study was funded in part by the European Research Council (ERC) (agreement No. 679058). The authors acknowledge the vivarium of the Champalimaud Centre for the Unknown, a facility of CONGENTO which is a research infrastructure co-financed by Lisboa Regional Operational Programme (Lisboa 2020), under the PORTUGAL 2020 Partnership Agreement through the European Regional Development Fund (ERDF) and Fundação para a Ciência e Tecnologia (Portugal), project LISBOA-01-0145-FEDER-022170.

Supplementary materials

Supplementary material associated with this article can be found, in the online version, at doi:10.1016/j.neuroimage.2021.117973.

References

Apšvalka, D., et al., 2015. Event-related dynamics of glutamate and BOLD effects measured using functional magnetic resonance spectroscopy (fMRS) at 3T in a repetition suppression paradigm. Neuroimage 118, 292–300. doi:10.1016/j.neuroimage.2015.06.015.

Archibald, J., et al., 2020. Metabolite activity in the anterior cingulate cortex during a painful stimulus using functional MRS. Sci. Rep. 10 (1), 1–12. doi:10.1038/s41598-020-76263-3, Nature Publishing Group UK.

van de Bank, B.L., et al., 2018. Is visual activation associated with changes in cerebral high-energy phosphate levels? Brain Struct. Funct. 223 (6), 2721–2731. doi:10.1007/s00429-018-1656-7, Springer Berlin Heidelberg.

Bednařík, P., et al., 2015. Neurochemical and BOLD responses during neuronal activation measured in the human visual cortex at 7 Tesla. J. Cereb. Blood Flow Metab. 35, 601–610. doi:10.1038/jcbfm.2014.233, January.

Bednařík, P., et al., 2018. Neurochemical responses to chromatic and achromatic stimuli in the human visual cortex. J. Cereb. Blood Flow Metab. 38 (2), 347–359. doi:10.1177/0271678x17695291.

Belle, J., Le, E., et al. 2002. 'A comparison of cell and tissue extraction techniques using high-resolution 1 H-NMR spectroscopy'. NMR Biomed. pp. 37–44. doi: 10.1002/nbm.740.

Betina Ip, I., et al., 2017. Combined fMRI-MRS acquires simultaneous glutamate and BOLD-fMRI signals in the human brain. Neuroimage 155, 113–119. doi:10.1016/j.neuroimage.2017.04.030, ElsevierDecember 2016.

Bezalel, V., Paz, R., Tal, A., 2019. NeuroImage inhibitory and excitatory mechanisms in the human cingulate-cortex support reinforcement learning : a functional proton magnetic resonance spectroscopy study. Neuroimage 184, 25–35. doi:10.1016/j.neuroimage.2018.09.016, Elsevier LtdMay 2018.

Boillat, Y., et al., 2019. Metabolite concentration changes associated with positive and negative BOLD responses in the human visual cortex: a functional MRS study at 7 Tesla. J. Cereb. Blood Flow Metab. doi:10.1177/0271678x19831022.

Boretius, S., et al., 2013. Halogenated volatile anesthetics alter brain metabolism as revealed by proton magnetic resonance spectroscopy of mice *in vivo*. Neuroimage 69, 244–255. doi:10.1016/j.neuroimage.2012.12.020, Elsevier Inc..

Bricault, S., et al., 2020. Image-guided neural activity manipulation with a paramagnetic drug. Nat. Commun. 1–6. doi:10.1038/s41467-019-13933-5, Springer US2020.

Buxton, R.B., 2013. The physics of functional magnetic resonance imaging (fMRI). Rep. Prog. Phys. 76 (9). doi:10.1088/0034-4885/76/9/096601.

Cao, P., et al., 2017. Simultaneous spin-echo and gradient-echo BOLD measurements by dynamic MRS. NMR Biomed. 30 (9), 1–9. doi:10.1002/nbm.3745.

Cleve, M., Gussew, A., Reichenbach, J.R., 2015. *In vivo* detection of acute pain-induced changes of GABA+ and Glx in the human brain by using functional 1H MEGA-PRESS MR spectroscopy. Neuroimage 105, 67–75. doi:10.1016/j.neuroimage.2014.10.042, Elsevier Inc..

Danbolt, N.C., 2001. Glutamate uptake. Prog. Neurobiol. 65, 1–105.

Frahm, J., et al., 1989. Localized high-resolution proton NMR spectroscopy using stimulated echoes: initial applications to human brain *in vivo*. Magn. Reson. Med. 9 (1), 79–93. doi:10.1002/mrm.1910090110.

Garwood, M., Delabarre, L., 2001. The return of the frequency sweep : designing adiabatic pulses for contemporary NMR. J. Magn. Reson. 153, 155–177. doi:10.1006/jmre.2001.2340.

Giapitzakis, I.A., et al., 2019. Investigation of the influence of macromolecules and spline baseline in the fitting model of human brain spectra at 9.4T. Magn. Reson. Med. 746–758. doi:10.1002/mrm.27467, June 2018.

Gil, R., Fernandes, F.F., Shemesh, N., 2021. Neuroplasticity-driven timing modulations revealed by ultrafast functional magnetic resonance imaging. Neuroimage 225, 117446. doi:10.1016/j.neuroimage.2020.117446, Elsevier Inc.September 2020.

Goense, J., Merkle, H., Logothetis, N.K., 2012. High-resolution fMRI reveals laminar differences in neurovascular coupling between positive and negative BOLD responses. Neuron 76 (3), 629–639. doi:10.1016/j.neuron.2012.09.019, Elsevier Inc..

Govindaraju, V., Young, K., Maudsley, A.A., 2000. Proton NMR chemical shifts and coupling constants for brain metabolites. NMR Biomed. 13 (3), 129–153.

Grandjean, J., et al., 2014. Optimization of anesthesia protocol for resting-state fMRI in mice based on differential effects of anesthetics on functional connectivity patterns. Neuroimage 102, 838–847.

Griffin, J.L., et al., 2002. Spectral profiles of cultured neuronal and glial cells derived from HRMAS 1 H NMR spectroscopy. NMR Biomed. 15, 375–384. doi:10.1002/nbm.792.

Gussew, A., et al., 2010. Time-resolved functional 1H MR spectroscopic detection of glutamate concentration changes in the brain during acute heat pain stimulation. Neuroimage 49 (2), 1895–1902. doi:10.1016/j.neuroimage.2009.09.007, Elsevier Inc..

Hendriks, A.D., et al., 2019. SNR optimized ^{31} P functional MRS to detect mitochondrial and extracellular pH change during visual stimulation. NMR Biomed. 1–10. doi:10.1002/nbm.4137, July 2018.

Jacobs, G.H., Williams, G.A., Fenwick, J.A., 2004. Influence of cone pigment coexpression on spectral sensitivity and color vision in the mouse. Vision Res. 44 (14), 1615–1622. doi:10.1016/j.visres.2004.01.016.

Just, N., et al., 2013. Characterization of sustained BOLD activation in the rat barrel cortex and neurochemical consequences. Neuroimage 74, 343–351. doi:10.1016/j.neuroimage.2013.02.042, Elsevier Inc..

Just, N., Faber, C., 2019. Probing activation-induced neurochemical changes using optogenetics combined with functional magnetic resonance spectroscopy (o-fMRS): a feasibility study in the rat primary somatosensory cortex. J. Neurochem. doi:10.1111/jnc.14799.

Just, N., Sonnay, S., 2017. Investigating the role of glutamate and GABA in the modulation of transthalamic activity: a combined fMRI-fMRS Study. Front. Physiol. 8. doi:10.3389/fphys.2017.00030, JAN.

Kingsley, P.B., 1994. Product operators, coherence pathways, and phase cycling. Part III: phase cycling. Concepts Magn. Reson. 7 (3), 167–192.

Kirov, I.I., Tal, A., 2020. Potential clinical impact of multiparametric quantitative MR spectroscopy in neurological disorders : a review and analysis. Magn. Reson. Med. 22–44. doi:10.1002/mrm.27912, April 2019.

Klose, U., 1990. *In vivo* proton spectroscopy in presence of eddy currents. Magn. Reson. Med. 14, 26–30.

Koush, Y., et al., 2019. Functional MRS with J-edited lactate in human motor cortex at 4 T. Neuroimage 184, 101–108. doi:10.1016/j.neuroimage.2018.09.008, Elsevier Ltd-September 2018.

Kühn, S., et al., 2016. Neurotransmitter changes during interference task in anterior cingulate cortex: evidence from fMRI-guided functional MRS at 3 T. Brain Struct. Funct. 221 (5), 2541–2551. doi:10.1007/s00429-015-1057-0.

Lein, E.S., et al., 2007. Genome-wide atlas of gene expression in the adult mouse brain. Nature 445 (7124), 168–176. doi:10.1038/nature05453.

Lin, Y., et al., 2012. Investigating the metabolic changes due to visual stimulation using functional proton magnetic resonance spectroscopy at 7 T. J. Cereb. Blood Flow Metab. 32 (8), 1484–1495. doi:10.1038/jcbfm.2012.33, Nature Publishing Group.

Logothetis, N.K., et al., 2001. Neurophysiological investigation of the basis of the fMRI signal. Nature 412, 150–157. doi:10.1038/35084005.

Logothetis, N.K., 2008. What we can do and what we cannot do with fMRI. Nature 453 (7197), 869–878. doi:10.1038/nature06976.
Logothetis, N.K., Wandell, B.A., 2004. Interpreting the BOLD signal. Annu. Rev. Physiol. 66 (1), 735–769. doi:10.1146/annurev.physiol.66.082602.092845.
Lopez-kolkovsky, A.L., Sebastien, M., Boumezbeur, F., 2016. Metabolite and macromolecule T1 and T2 relaxation times in the rat brain *in vivo* at 17.2T. Magn. Reson. Med. 75, 503–514. doi:10.1002/mrm.25602.
Magistretti, P.J., Allaman, I., 2015. A cellular perspective on brain energy metabolism and functional imaging. Neuron 86 (4), 883–901. doi:10.1016/j.neuron.2015.03.035, Elsevier Inc..
Mangia, S., Tkáč, I., Logothetis, N.K., et al., 2007. Dynamics of lactate concentration and blood oxygen level-dependent effect in the human visual cortex during repeated identical stimuli. J. Neurosci. Res. 85, 3340–3446. doi:10.1002/jnr, May.
Mangia, S., Tkáč, I., Gruetter, R., et al., 2007. Sustained neuronal activation raises oxidative metabolism to a new steady-state level: evidence from 1H NMR spectroscopy in the human visual cortex. J. Cereb. Blood Flow Metab. 27 (5), 1055–1063. doi:10.1038/sj.jcbfm.9600401.
Marín, O., 2012. Interneuron dysfunction in psychiatric disorders. Nat. Rev. Neurosci. 107–120. doi:10.1038/nrn3155, January.
Martínez-Maestro, M., Labadie, C., Möller, H.E., 2018. Dynamic metabolic changes in human visual cortex in regions with positive and negative blood oxygenation level-dependent response. J. Cereb. Blood Flow Metab. doi:10.1177/0271678x18795426.
May, P.J., 2006. The mammalian superior colliculus : laminar structure and connections. Prog. Brain Res. 151, 321–378. doi:10.1016/S0079-6123(05)51011-2.
Mekle, R., et al., 2017. Detection of metabolite changes in response to a varying visual stimulation paradigm using short-TE 1H MRS at 7 T. NMR Biomed. 30 (2), 1–9. doi:10.1002/nbm.3672.
Mlynárik, V., et al., 2008. H NMR spectroscopy of rat brain *in vivo* at 14 . 1 Tesla : improvements in quantification of the neurochemical profile. J. Magn. Reson. 194, 163–168. doi:10.1016/j.jmr.2008.06.019.
Mulkern, R., Bowers, J., 1994. Density matrix calculations of AB spectra from multipulse sequences : quantum mechanics meets *in vivo* spectroscopy. Concepts Magn. Reson. 6, 1–23.
Mullins, P.G., 2018. Towards a theory of functional magnetic resonance spectroscopy (fMRS): a meta-analysis and discussion of using MRS to measure changes in neurotransmitters in real time. Scand. J. Psychol. 59 (1), 91–103. doi:10.1111/sjop.12411.
Niranjan, A., et al., 2016. 'fMRI mapping of the visual system in the mouse brain with interleaved snapshot GE-EPI. Neuroimage 139, 337–345. doi:10.1016/j.neuroimage.2016.06.015, The Authors.
Palombo, M., Ligneul, C., Valette, J., 2017. Modeling diffusion of intracellular metabolites in the mouse brain up to very high diffusion-weighting : diffusion in long fibers (Almost) accounts for non-monoexponential attenuation. Magn. Reson. Med. 350, 343–350. doi:10.1002/mrm.26548, November 2016.
Pijnappel, W.W.F, et al., 1992. SVD-based quantification of magnetic resonance signals. J. Magn. Reson. (1969) 97 (1), 122–134. doi:10.1016/0022-2364(92)90241-X.
Polimeni, J.R., et al., 2010. Laminar analysis of 7 T BOLD using an imposed spatial activation pattern in human V1. Neuroimage 52 (4), 1334–1346. doi:10.1016/j.neuroimage.2010.05.005, Elsevier Inc..
Prichard, J., et al., 1991. Lactate rise detected by 1H NMR in human visual cortex during physiologic stimulation. Proc. Natl. Acad. Sci. 88 (July), 5829–5831.
Provencher, S.W., 1993. Estimation of metabolite concentrations from localized *in vivo* proton NMR spectra. Magn. Reson. Med. 30, 672–679.
Robinson, M., et al., 1987. Hydrolysis of the brain dipeptide N-Acetyl-L-aspartyl-L-glutamate. J. Biol. Cherm. 262 (30), 14498–14506.
Roth, B.L., 2016. DREADDs for neuroscientists. Neuron 89 (4), 683–694. doi:10.1016/j.neuron.2016.01.040, Elsevier Ltd.
Schaller, B., et al., 2013. Net increase of lactate and glutamate concentration in activated human visual cortex detected with magnetic resonance spectroscopy at 7 tesla. J. Neurosci. Res. 91 (8), 1076–1083. doi:10.1002/jnr.23194.
Seuwen, A., et al., 2015. Metabolic changes assessed by MRS accurately re fl ect brain function during drug-induced epilepsy in mice in contrast to fMRI-based hemodynamic readouts. Neuroimage 120, 55–63.
Seuwen, A., et al., 2019. Functional spectroscopic imaging reveals specificity of glutamate response in mouse brain to peripheral sensory stimulation. Sci. Rep. 9 (1), 1–9. doi:10.1038/s41598-019-46477-1, Springer US.
Sonnay, S., et al., 2018. Astrocytic and neuronal oxidative metabolism are coupled to the rate of glutamate–glutamine cycle in the tree shrew visual cortex. Glia 66 (3), 477–491. doi:10.1002/glia.23259.
Sonnay, S., Duarte, J.M.N., Just, N, 2017. Lactate and glutamate dynamics during prolonged stimulation of the rat barrel cortex suggest adaptation of cerebral glucose and oxygen metabolism. Neuroscience 346, 337–348. doi:10.1016/j.neuroscience.2017.01.034.
Stanley, J.A., Raz, N., 2018. Functional magnetic resonance spectroscopy: the "new" MRS for cognitive neuroscience and psychiatry research. Front. Psychiatry 9. doi:10.3389/fpsyt.2018.00076, MAR.
Tannüs, A., Garwood, M., 1996. Improved performance of frequency-swept pulses using offset-independent adiabaticity. J. Magn.Reson.- Series A 120 (1), 133–137. doi:10.1006/jmra.1996.0110.
Taylor, R., Neufeld, R.W.J., et al., 2015. Functional magnetic resonance spectroscopy of glutamate in schizophrenia and major depressive disorder: anterior cingulate activity during a color-word Stroop task. NPJ Schizophr. 1 (1). doi:10.1038/npjschz.2015.28, Nature Publishing Group.
Taylor, R., Schaefer, B., et al., 2015. Increased glutamate levels observed upon functional activation in the anterior cingulate cortex using the Stroop Task and functional spectroscopy. Neuroreport 26 (3), 107–112. doi:10.1097/WNR.0000000000000309.
Tkáč, I., et al., 1999. *In vivo* 1 H NMR spectroscopy of rat brain at 1 ms echo time. Magn. Reson. Med. 41, 649–656.
Tkáč, I., et al., 2004. Highly resolved *in vivo* 1 H NMR spectroscopy of the Mouse Brain at 9 . 4 T. Magn. Reson. Med. 484, 478–484. doi:10.1002/mrm.20184, December 2003.
Tsai, G., et al., 1993. Immunocytochemical distribution of N-acetylaspartylglutamate in the rat forebrain and glutamatergic pathways. J. Neuroanat. 6, 277–292.
Urenjak, J., et al., 1993. Proton nuclear magnetic resonance spectroscopy identifies different neural cell types. J. Neurosci. 13 (3), 981–989.
Vijayakumari, A.A., et al., 2020. Glutamatergic response to a low load working memory paradigm in the left dorsolateral prefrontal cortex in patients with mild cognitive impairment: a functional magnetic resonance spectroscopy study. Brain Imaging Behav. 14 (2), 451–459. doi:10.1007/s11682-019-00122-7.
Vincent, M., et al., 2021. Characterizing extracellular diffusion properties using diffusion-weighted MRS of sucrose injected in mouse brain. NMR Biomed. 1–16. doi:10.1002/nbm.4478, January.
Volovyk, O., Tal, A., 2020. Increased glutamate concentrations during prolonged motor activation as measured using functional magnetic resonance spectroscopy at 3T. Neuroimage 223, 117338. doi:10.1016/j.neuroimage.2020.117338, Elsevier Inc.September.
Wang, L., et al., 2010. Visual receptive field properties of neurons in the superficial superior colliculus of the mouse. J. Neurosci. 30 (49), 16573–16584. doi:10.1523/jneurosci.3305-10.2010.
Wang, R., et al., 1996. Expression of alpha2-adrenergic receptor subtypes in the mouse brain: evaluation of spatial and temporal information imparted by 3 kb of 5' regulatory sequence for the a 2AAR-receptor gene in transgenic animals. Neuroscience 74 (1), 199–218.
Yablonskiy, D.A., Haacke, E.M., 1994. Theory of NMR signal behavior in magnetically inhomogeneous tissues: the static dephasing regime. Magn. Reson. Med. 32 (6), 749–763. doi:10.1002/mrm.1910320610.
Zhao, S., et al., 2011. Cell type-specific channelrhodopsin-2 transgenic mice for optogenetic dissection of neural circuitry function. Nat. Methods 8 (9), 745–755. doi:10.1038/nmeth.1668.
Zhu, X.H., Chen, W., 2001. Observed BOLD effects on cerebral metabolite resonances in human visual cortex during visual stimulation: a functional 1H MRS study at 4 T. Magn. Reson. Med. 46 (5), 841–847. doi:10.1002/mrm.1267.abs.